



Classification of urban areas from GeoEye-1 imagery through texture features based on Histograms of Equivalent Patterns

Manuel A. Aguilar, Antonio Fernández, Fernando J. Aguilar, Francesco Bianconi & Andrés García Lorca

To cite this article: Manuel A. Aguilar, Antonio Fernández, Fernando J. Aguilar, Francesco Bianconi & Andrés García Lorca (2016) Classification of urban areas from GeoEye-1 imagery through texture features based on Histograms of Equivalent Patterns, European Journal of Remote Sensing, 49:1, 93-120, DOI: [10.5721/EuJRS20164906](https://doi.org/10.5721/EuJRS20164906)

To link to this article: <https://doi.org/10.5721/EuJRS20164906>



© 2016 The Author(s). Published by Taylor & Francis.



Published online: 17 Feb 2017.



Submit your article to this journal [↗](#)



Article views: 377



View Crossmark data [↗](#)



Citing articles: 5 View citing articles [↗](#)



Classification of urban areas from GeoEye-1 imagery through texture features based on Histograms of Equivalent Patterns

Manuel A. Aguilar^{1*}, Antonio Fernández², Fernando J. Aguilar¹,
Francesco Bianconi³ and Andrés García Lorca⁴

¹Department of Engineering, University of Almería, Ctra Sacramento s/n, 04120, Almería, Spain

²Department of Engineering Design, University of Vigo, Campus Universitario, 36310, Vigo, Spain

³Department of Engineering, Università degli Studi di Perugia, Via G. Duranti 93, 06125, Perugia, Italy

⁴Department of Geography, University of Almería, Ctra Sacramento s/n, 04120, Almería, Spain

*Corresponding author, e-mail address: maguilar@ual.es

Abstract

A family of 26 non-parametric texture descriptors based on Histograms of Equivalent Patterns (HEP) has been tested, many of them for the first time in remote sensing applications, to improve urban classification through object-based image analysis of GeoEye-1 imagery. These HEP descriptors have been compared to the widely known texture measures derived from the gray-level co-occurrence matrix (GLCM). All the five finally selected HEP descriptors (Local Binary Patterns, Improved Local Binary Patterns, Binary Gradient Contours and two different combinations of Completed Local Binary Patterns) performed faster in terms of execution time and yielded significantly better accuracy figures than GLCM features. Moreover, the HEP texture descriptors provided additional information to the basic spectral features from the GeoEye-1's bands (R, G, B, NIR, PAN) significantly improving overall accuracy values by around 3%. Conversely, and in statistic terms, strategies involving GLCM texture derivatives did not improve the classification accuracy achieved from only the spectral information. Lastly, both approaches (HEP and GLCM) showed similar behavior with regard to the training set size applied.

Keywords: GeoEye-1, OBIA, texture, histograms of equivalent patterns.

Introduction

Since the first very high resolution (VHR) satellite called IKONOS was successfully launched in 1999, images with spatial resolutions less than 1 m are constantly acquired over the earth surface. GeoEye-1 (GE1) is currently the second world's highest spatial resolution commercial Very High Resolution (VHR) Earth Observation satellite, in both panchromatic (PAN) and multispectral (MS) products. This optical satellite, successfully launched in late 2008, is able to capture images of the Earth surface with 0.41 m (PAN) and 1.65 m (MS) ground sample distance (GSD) at nadir. GE1 can

simultaneously capture the PAN band (spectral range from 450 to 800 nm) and four MS bands such as Blue (B: 450 to 510 nm), Green (G: 510-580 nm), Red (R: 655-690 nm) and Near Infrared (NIR: 780-920 nm). It is worth noting that the higher geometric detail of a PAN image and the useful color information of a lower resolution MS image (four bands) can be integrated to produce a final pan-sharpened MS image with high spatial resolution by applying image fusion techniques [Sarp, 2014; Nikolakopoulos and Oikonomidis, 2015].

With the availability of pan-sharpened VHR satellite imagery, classification of small scale manmade structures in urban environments have become of great interest. In the last decade, Object-Based Image Analysis (OBIA) has proved to be an effective approach to deal with this problem [Carleer and Wolff, 2006; Blaschke, 2010; Lu et al., 2010; Myint et al., 2011; Weng, 2012; Gianinetto et al., 2014]. OBIA does not use individual pixels but pixel groups representing meaningful segments (or objects), which have been segmented according to different criteria before the classification stage is carried out. At this point, and regarding remote sensing image analysis, it should be clearly stated that much of the work referred to as OBIA has been originated around the software known as eCognition (Trimble, Sunnyvale, California, United States). Indeed, about 50%-55% of the papers related to OBIA are based on this package [Blaschke, 2010].

With the advent of VHR satellite imagery, real world objects or regions that were previously represented by only one or two pixels consist now of many pixels. Therefore, techniques that take into account the existing spatial relations between image pixels within an image region have good chance to improve classification accuracy. Texture analysis is one of the most interesting and extended approaches for extracting this spatial structure. In fact, texture analysis is playing an increasingly important role in remote sensing image processing, principally motivated by the fact that it can provide supplementary information about image properties. The applications of texture extraction in remote sensing image classifications can be traced back to 1970s [Li et al., 2014]. Perhaps the most popular and widely used approach to extract image textural information are the second order texture features based on the so-called gray-level co-occurrence matrix (GLCM) proposed by Haralick et al. [1973]. The inclusion of texture features seems to significantly improve classification accuracy of satellite images [Puissant et al., 2005; Carleer and Wolff, 2006; Agüera et al., 2008; Murray et al., 2010; Ozdemira and Karnieli, 2011; Stumpf and Kerle, 2011; Eckert 2012; Longbotham et al., 2012; Aguilar et al., 2013, Gianinetto et al., 2014]. Many feature extraction algorithms based on the GLCM have been proposed in the literature. For example, the GLCM model has been recently extended to three-dimensional space through the volumetric GLCM (VGLCM) [Tsai et al., 2007; Su et al., 2014; Su et al., 2015], which is specifically designed for multispectral or hyperspectral imagery. In addition to the classical GLCM, other techniques to extract spatial information have been proposed and tested in the literature, including Markov random fields [Lorette et al., 2000; Zhao et al., 2007], Gabor filters [Clausi and Deng, 2005; Bianconi and Fernández, 2007], fractals [Parrinello and Vaughan, 2002], Moran's I [Su et al., 2008] or wavelet [Myint et al., 2004; Huang and Zhang, 2012].

Texture classification has rapidly evolved during the last 20 years and many new

approaches have been proposed. Several new texture descriptors such as Local Binary Patterns (LBP) [Ojala et al., 2002], Improved Local Binary Patterns (ILBP) [Jin et al., 2004], Binary Gradient Contours (BGC) [Fernández et al., 2011] or Completed Local Binary Patterns (CLBP) [Guo et al., 2010], have been described in literature. The vast majority of the new available descriptors have been presented in the field of computer vision and pattern recognition and many have never tested in remote sensing applications. Of these, LBP have received attention in recent years for the segmentation and classification of airborne or satellite imagery [Lucieer et al., 2005; Li et al., 2010; Mdakane and Van den Bergh, 2012; Musci et al., 2013; Li et al., 2015]. Also CLBP was tested by Malek et al. [2015] in a paper focused on palm tree detection from unmanned aerial vehicles images.

Recently Fernández et al. [2013] demonstrated that many of the texture descriptors which characterize a texture image through the probability of occurrence of the patterns associated to a neighborhood of given size and shape belong to a general framework for texture analysis which they referred to as the HEP (Histograms of Equivalent Patterns). The HEP is based on partitioning the feature space associated to image patches of predefined shape and size. The partition is based on a priori suitable local or global functions of the pixels' intensities [Bianconi and Fernández, 2014].

As already stated, second-order statistics derived from the GLCM are the most popular texture descriptors used in remote sensing. Moreover, eCognition is considered a standard in OBIA software working with VHR satellite imagery. Therefore, the classification accuracy attained by means of GLCM derivatives computed and classified into eCognition environment can be considered as a benchmark for other texture descriptors. On that basis, the main contribution of this paper is the performance comparison, in terms of computation time and classification accuracy, of GLCM features (classical approach) and a set of HEP texture descriptors for supervised object-based classification. To the best of our knowledge, this is the first study in which the HEP framework is tested in remote sensing applications. In fact, many of the descriptors included in HEP had never been used in VHR satellite imagery classification. The interaction between the texture descriptors tested in urban environments from VHR GE1 imagery and the number of samples used for training the classifier (training set size) is also studied. In addition, it will be estimated the increase in classification accuracy that GLCM and HEP texture features extracted from the PAN channel can achieve when combined with basic spectral information contained in the R, G, B, PAN and NIR bands from both pan-sharpened and PAN images.

Study site

The study area comprises 17 ha in the seaside village of Villaricos, province of Almería, Southern Spain (Fig. 1). The working area is centered on the WGS84 coordinates (Easting and Northing) of 609,007 m and 4,123,230 m. Its urban landscape presents high heterogeneity, with mixing old buildings and new housing developments, and therefore represents a challenging dataset for object-based classification.

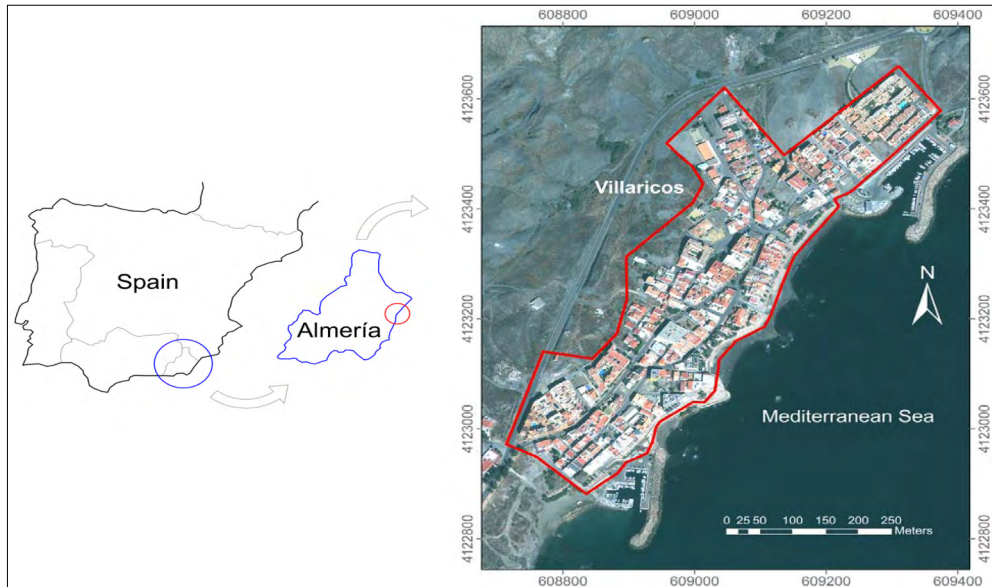


Figure 1 - Location of the study site. The working area has been delimited by the red polygon. Coordinate system: WGS84 UTM zone 30N.

GeoEye-1 data

A map-projected GE1 Geo (now known as Ortho-Ready Standard) bundle image, simultaneously recording the PAN and the four MS bands, was acquired on 29 September 2010. The original product presented an off-nadir viewing angle of 20.6° , 16 bits per pixel (without dynamic range adjustment) and a spatial resolution of 0.5 m and 2 m in PAN and MS mode respectively. The corresponding pan-sharpened image, presenting a 0.5 m GSD and containing the whole spectral information coming from the MS image (4-bands), was attained by using the PANSARP algorithm included in Geomatica v. 2012 (PCI Geomatics, Richmond Hill, Ontario, Canada). Finally, three 0.5 m GSD orthoimages (two PAN with 8-bit and 16-bit dynamic range, and one 16-bit pan-sharpened orthoimage) were computed by using OrthoEngine, the photogrammetric module of Geomatica software. Both orthoimages were obtained through the Rational Function model with zero order transformation in image space by using very accurate ancillary data such as 7 ground control points (GCPs) measured by DGPS and a LiDAR (Light Detection and Ranging) derived digital elevation model (DEM). These orthoimages presented a two-dimensional root mean squared error ($RMSE_{2D}$) of 0.46 m estimated from 75 independent check points [Aguilar et al., 2012].

Methodology

Image segmentation is a crucial step of OBIA that splits an image into separated and homogeneous regions or image objects (IOs) on which later process will be applied. For this task, a widely known multiresolution segmentation algorithm included in eCognition Developer 8 was used. For achieving the final segmentation, multiresolution algorithm

was applied in two steps. A scale value of 20 at pixel level was used for the first step and, secondly, a scale value of 70 was applied on the first segmentation level scale. The segmentation was always computed by taking into account the four equally-weighted bands corresponding to the pan-sharpened orthoimage. Furthermore, compactness criterion was assigned a weight of 0.5 and shape value was fixed at 0.3 (i.e. weight of color = 0.7).

The segmentation parameters were determined based on expert judgment and visual interpretation through trial-and-error. As a result, 2723 IOs which match well the feature boundaries of the main land covers within the study area were obtained [Aguilar et al., 2013]. Therefore, segmentation step assured pure objects (i.e. grouping pixels belonging to an only class) to later classify them and assessing the final classification accuracy by using a ground truth also based on that segmentation.

Ground reference

A ground reference was carried out into GIS environment by careful visual inspection of separate data sources. More details can be found in Aguilar et al. [2013]. The IOs resulting from the segmentation process were manually checked and finally classified into nine target classes (Tab. 1), thereby generating the reference map. It is worth noting that the proposed accuracy assessment, based on the ground reference map, exactly matched the previously segmented IOs and so contributed to artificially removing the potential segmentation errors, i.e. extra pixels and lost pixels defined by Marpu et al. [2010]. In this sense, under-segmentation (splitting up the image into too few objects) was avoided by discarding from the ground reference map those segments not being pure class IOs. By applying this rule, 1886 out of the initial 2723 IOs were visually identified as meaningful objects (Tab. 1). A subset of 941 well-distributed IOs were selected to carry out the training phase, whereas the remaining 945 IOs, also evenly distributed within the working area, were taken aside to cope with the validation phase. Total surface areas occupied by IOs for each class over the final ground reference map, as well as their mean and standard deviation (SD), are also depicted in Table 1.

Table 1 - IOs after GE1 segmentation and manual classification related to the target classes.

Class	No. IOs	Area (m ²)			Validation IOs	Training IOs
		Total Area	Mean	SD		
Red buildings	298	22217	74.55	51.62	149	149
White buildings	558	17034.25	30.53	37.57	279	279
Grey buildings	68	5279.5	77.64	57.11	34	34
Other buildings	55	3086.25	56.11	34.04	28	27
Shadows	477	21600	45.28	63.59	239	238
Vegetation	194	17192.5	88.62	88.13	97	97
Bare soil	93	15464	166.28	126.84	47	46
Roads	72	15720.5	218.34	161.99	36	36
Streets	71	7317.75	103.07	109.06	36	35

The manually assigned reference map including both training and validation subsets (i.e. 1886 IOs) based on previous segmentation is shown in Figure 2a, where the four classes related to buildings (i.e. red, white, grey and others buildings) are presented as only one aggregated class named Buildings. It should be noted that both the IOs used as training samples (Fig. 2b) and those employed to carry out the accuracy assessment were always meaningful object.

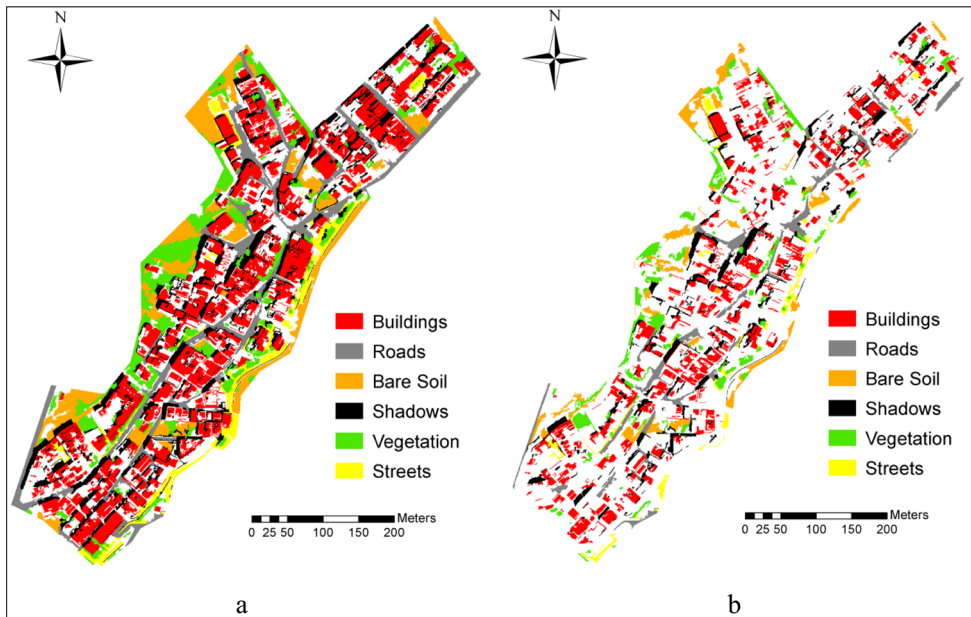


Figure 2 - Manually assigned reference map including (a) both training and validation subsets and (b) map depicting the distribution of the IOs used as training samples.

Classifier and selection of training areas

The classification algorithm based on the Nearest Neighbour (NN) rule is simple to implement and generally performs good results with carefully chosen features. Thus, all the classification tests were carried out by using the NN rule for both GLCM and HEP according to the pursued goal of comparison purpose.

On one hand, the classical tests involving GLCM, including classification stage, were entirely computed within eCognition Developer 8. The NN classifier implemented in eCognition uses a fuzzy approach defined by membership functions [Baatz et al., 2004]. It returns a membership value of between zero and one based on the image object feature space distance to its nearest neighbor. The membership value takes a value of one if the train and test feature vectors are coincident. Otherwise the membership value is computed considering the separation to the nearest training samples [Definiens, 2009]. On the second hand, the 1-NN with L1 distance classifier implemented in MATLAB® R2008b is used to test the HEP descriptors.

Regarding the training areas, four random repetitions each containing 5, 10, 15 and 20% of

the total number of IOs were extracted from the whole training subset, resulting in a total of 16 training sets [Aguilar et al., 2013]. Table 2 depicts the number of IOs chosen for the classifier training stage.

Table 2 - Number of IOs used for training regarding training size and target class (four replicates for every training set).

Class	5% Training	10% Training	15% Training	20% Training
Red buildings	15	30	45	60
White buildings	28	56	84	112
Grey buildings	4	7	11	14
Other buildings	3	6	11	15
Shadows	24	48	72	96
Vegetation	10	20	30	39
Bare soil	5	10	14	19
Roads	4	8	11	15
Streets	4	8	11	15

GLCM texture descriptors tested

In most practical remote sensing applications involving VHR satellite images only GLCM derivatives are used as texture descriptors. Thus, in order to have a benchmark for other texture descriptors we decided to run the whole process of computing GLCM and classifying the image into eCognition environment.

Second-order statistics derived from the GLCM describe changes in gray-level values of pixels and relationships between pixel pairs in a given area [Haralick et al., 1973]. Regarding pixel-based analysis, texture is extracted from moving windows what can produce boundary problems. That is, windows can straddle the boundary between two landscape features and potentially different textures [Ferro and Warner, 2002]. However, when texture is calculated from segmented imagery, the boundary problem is minimized because the segments are relatively homogenous and texture is calculated for all pixels belonging to an image object.

In this study only five out of the 14 GLCM texture features originally proposed by Haralick et al. [1973] were considered, due to both the strong correlation frequently reported between many of them [Baraldi and Pannigiani, 1995; Laliberte and Rango, 2009] and their large computational burden. The five selected features were contrast (CON), entropy (ENT), mean (MEAN), standard deviation (SD) and correlation (COR). The same subset of GLCM texture features was selected by Stumpf and Kerle [2011] working on a similar OBIA workflow.

In eCognition software, Haralick texture features are calculated for all pixels contained in an image object. Pixels directly bordering the image object (surrounding pixels with a distance of 1) are additionally taken into account to reduce border effects. Rotation-invariant GLCM features are achieved by summing up the four directional matrices (i.e., 0°, N-S, 45°, NE-SW, 90°, E-W and 135°, SW-NE). All the five GLCM features were computed from the

16-bit PAN GE1 orthoimage owing to it would be probably the way followed by a common user. Anyway, the calculation of GLCM textures in eCognition is independent of the data bit-depth due to the fact that the dynamic range is interpolated to 8-bit before evaluating the co-occurrence matrix. All available information about how eCognition computes texture after Haralick can be found in Definiens [2009].

HEP texture descriptors tested

The HEP family represents in this work a set of alternative texture descriptors to the classical GLCMs. In order to understand the basic concept of HEP framework, the reader should be in mind that the texture structure of an image can be attained by detecting different grey-scale patterns, the probability of which can be estimated through a histogram. In this way and for the sake of clarity, the following example is presented. The number of different 3×3 grey-scale patterns would be 256^9 considering an 8-bit PAN image. In this case, the ultra-high dimensional histogram would provide an unreliable estimation of the underlying texture structure. In this regard, any method belonging to the HEP deals with this problem by, firstly, defining a partition of the pattern space into classes of equivalent patterns being the number of classes equal to the dimensionality of the method, and, secondly, by merging the histogram bins of the equivalent ones [Fernández et al., 2013]. So, every HEP descriptor will be based in a suitable function f (the kernel function) in order to reduce the dimension of the histogram patterns. Details of some HEP descriptors can be found below.

For example, in the 3×3 domain (Eq. [1]) the Local Binary Patterns (LBP) operator [Ojala et al., 2002] thresholds the eight peripheral pixels of the neighbourhood, I_j ($j \in \{0, 1, \dots, 7\}$) at the value of the central pixel, I_c , thus defining a set of 2^8 possible binary patterns, significantly reducing the aforementioned 256^9 original patterns. In this case, Equation [2] shows the kernel function for LBP, being $\xi(x)$ the binary thresholding function (Eq. [3]).

$$\mathbf{x} = \begin{bmatrix} I_7 & I_6 & I_5 \\ I_0 & I_c & I_4 \\ I_1 & I_2 & I_3 \end{bmatrix} \quad [1]$$

$$f_{LBP}(\mathbf{x}) = \sum_{j=0}^7 2^j \xi(I_j - I_c) \quad [2]$$

$$\xi(x) = \begin{cases} 1, & \text{if } x \geq 0 \\ 0, & \text{if } x < 0 \end{cases} \quad [3]$$

Other HEP texture descriptor tested in this work is the first Binary Gradient Contours (BGC1) proposed by Fernández et al. [2011]. This descriptor is based on pairwise comparison of adjacent pixels belonging to a closed path traced along the periphery of the 3×3 neighbourhood (hence the name contours). In the case of BGC1 the pixels that define

the path are: $\{0, 1, \dots, 7, 0\}$ (Eq. [1]), therefore the corresponding couples from which the binary values are extracted are: $\{(0, 1), (1, 2), \dots, (7, 0)\}$. BGC1 generates $(2^8 - 1)$ possible different patterns, since the all 0s pattern is impossible by definition. The kernel function of BGC1 is reported in Equation [4].

$$f_{BGC1}(\mathbf{x}) = \sum_{j=0}^7 2^j \xi(I_j - I_{(j+1) \bmod 8}) - 1 \quad [4]$$

The improved local binary patters (ILBP) descriptor [Jin et al., 2004] are based on an idea similar to LBP, the only difference is that the whole 3×3 neighbourhood is thresholded by its average grey-scale value. This gives $(2^9 - 1)$ possible binary patterns (the all 0s pattern is not possible by definition hence the -1). The kernel function is expressed in Equation 5 where \bar{S} is the average grey-scale value over the neighbourhood (Eq. [6]).

$$f_{ILBP}(\mathbf{x}) = 2^8 \xi(I_c - \bar{S}) + \sum_{j=0}^7 2^j \xi(I_j - S) - 1 \quad [5]$$

$$\bar{S} = \frac{1}{9} \left(I_c + \sum_{j=0}^7 I_j \right) \quad [6]$$

On a different note, Completed Local Binary Patterns (CLBP) are actually combinations of the three basic operators such as CLBP_Sign (CLBP_S), CLBP_Magnitude (CLBP_M) and CLBP_Center (CLBP_C) described by Guo et al. [2010]. CLBP_S is just an alias for LBP, only changing the values of the binary thresholding function (Eq. [3]) for -1 when $x < 0$. CLBP_C thresholds the central pixel at the average grey value of the whole image (\bar{I}), and therefore generates only two binary patterns. Bearing in mind that the whole image size is representing by a $M \times N$ matrix, the kernel function is shown in Equation [7], being \bar{I} defined in Equation [8].

$$f_{CLBP_C}(\mathbf{x}) = \xi(I_c - \bar{I}) \quad [7]$$

$$\bar{I} = \frac{\sum_{m=1}^M \sum_{n=1}^N I_{m,n}}{MN} \quad [8]$$

CLBP_M considers the possible binary patterns that are defined by the absolute difference between the gray value of a pixel in the periphery and that of the central pixel when thresholded with a global parameter (Eq. [9]), where \tilde{I} is the average value of the difference

in grey value between a pixel in the periphery and the central pixel (Eq. [10]).

$$f_{CLBP_M}(\mathbf{x}) = \sum_{j=0}^7 2^j \xi(|I_j - I_c| - \tilde{I}) \quad [9]$$

$$\tilde{I} = \frac{\sum_{m=2}^{M-1} \sum_{n=2}^{N-1} \sum_{i=-1}^1 \sum_{j=-1}^1 |I_{m-i, n-j} - I_{m,n}|}{8(M-2)(N-2)} \quad [10]$$

It is noteworthy that CLBP_MxC descriptor used in this work represents the combination of CLBP_M and CLBP_C, i.e., a joint 2D histogram is computed. In the same way, CLBP_S_MxC is the concatenation of CLBP_S and CLBP_MxC, i.e., first the histograms are calculated separately for later being concatenated together.

The HEP is a family of conceptually simple, easy to implement and reasonably fast texture descriptors. Fernández et al. [2013] described a general framework for texture analysis based on HEP including around 40 texture descriptors for 256 levels of digital number images and using a 3×3 square neighbourhood (the source code implemented in MATLAB® R2008b is available in <http://webs.uvigo.es/antfdez/downloads.html>). The unambiguous mathematical definition of the HEP descriptors carried out by Fernández et al. [2013] allowed us to test 26 non-parametric ones on our 8-bit PAN orthoimage from GE1 by using the aforementioned 1-NN with L1 distance classifier. After analyzing the first results, we selected five of the tested non-parametric texture descriptors: LBP, ILBP, BGC1, CLBP_MxC and CLBP_S_MxC, which have been conveniently explained throughout this section.

Fuzzy fusion of spectral and texture features for image object classification

The main goal of this section is to integrate the hypothetically complementary information provided by spectral and texture features to improve the final OBIA classification accuracy. In fact, combining information from different feature vectors or classifiers represents an important research line in the field of image classification [Kittler et al., 1998; Segl et al., 2003; Permuter et al., 2006; Deselaers et al., 2010]. In theory, the integration of different and independent sources of information should improve the classification accuracy [Kittler et al., 1998]. In this sense, different sources of information are combined by voting rules, statistical techniques, belief functions, Dempster-Shafer evidence theory and other fusion schemes. It is beyond the scope of this paper the search of the best fusion scheme for our particular case. On the contrary, this section only tries to demonstrate that it is possible to significantly improve the final OBIA accuracy classification results by fusing the object information extracted from both spectral and texture features. Herein we investigated two different fusion strategies: 1) concatenation of features vector, and 2) fusion of a-posteriori class probabilities through Bayesian average. These two approaches are described here below.

1) Concatenation of feature vectors

This is the usual approach in remote sensing when the fused feature vectors present a low and similar dimension. This is the case of the fusion of the Haralick texture features and the basic spectral features used in this work (i.e. R, G, B, NIR and PAN bands from the GE1 orthoimages), where a NN supervised classification is carried out onto eCognition by simply concatenating the feature vectors. The following combinations were tested:

- i) RGBNP_eCog (dimension=5): basic spectral features from GE1 imagery which refers to the mean DN values for every previously segmented object corresponding to the R, G, B, NIR and PAN bands;
- ii) +GLCM_MEAN (dimension=6): fusion of the basic spectral features and GLCM Mean;
- iii) +GLCM_SD (dimension=6): fusion of the basic spectral features and GLCM Standard Deviation;
- iv) +GLCM_ENT (dimension=6): fusion of the basic spectral features and GLCM Entropy;
- v) +GLCM_CON (dimension=6): fusion of the basic spectral features and the GLCM Contrast texture descriptor;
- vi) +GLCM_COR (dimension=6): fusion of the basic spectral features and GLCM Correlation;
- vii) +5_GLCMs (dimension=10): fusion of the basic spectral features and the five GLCM-based texture descriptors.

2) Fusion of a-posteriori class probabilities through Bayesian average

It is not recommendable to concatenate HEP texture descriptors and spectral features due to the high dimension of HEP mappings (ranging from 255 to 768 for the five finally selected mappings) as compared to the low dimension of the spectral feature vector for GE1 (only five features corresponding to the spectral digital values of R, G, B, NIR and PAN bands). To overcome this problem we propose Bayesian averaging [Ruta and Gabrys, 2000].

The method can be applied to feature fusion provided that the output of the NN classifier is expressed as posterior probabilities. In this way, this means a fuzzy approach where it is necessary to estimate the posterior probabilities that an input object or segment with a feature vector X may belong to the target class w_i (initially nine in our tests), i.e., $P(X \in w_i)$ for $i=1$ to M , being M the number of target classes. In our approach, posterior probabilities are computed through the inverse of L1 distance. This implies computing the L1 distance between every object to classify and the nearest training sample (1-NN approach) for each target class (d_i). A normalized kernel is applied to ensure that the membership values of each object to classify to belong to one of the target classes sum 1. Furthermore, a constant shift term ($k = 0.05$ in our case) is added to the L1 distance for avoiding singularities when the training sample and the object to classify present just the same feature vector and so the distance between them turns out to be zero (Eqs. [11] and [12]).

$$P(X \in w_i) = \frac{1}{k + d_i} \Big/ \sum_{j=1}^M \frac{1}{k + d_j}; \quad i = 1 \text{ to } M \quad [11]$$

$$\sum_{\forall i} P(X \in w_i) = 1; \quad i = 1 \text{ to } M \quad [12]$$

These posterior probabilities are separately computed for every feature vector involved in the fusion process. Thus, a given input pattern extracted from an object receives L classification labels with posterior probabilities depending on the feature vectors used, being L the number of different feature spaces to be fused. In the context of expert fusion, it would be equivalent to fusing the opinion of several experts. The final classification is performed by applying the Bayesian average criterion, i.e., the object input pattern X is assigned to the target class for which $P_{average}(X \in w_i)$ presents the maximum value according to the Equation [13].

$$P_{average}(X \in w_i) = \frac{1}{L} \sum_{j=1}^L P_j(X \in w_i); \quad i=1 \text{ to } M \quad [13]$$

The previously described Bayesian Average fusion scheme based on 1-NN L1 classifier was implemented in MATLAB®. In an analogous way to that used in the GLCM case, the following strategies to combine information from both the spectral and the previously mentioned group of five HEP texture descriptors were tested:

- i) RGBNP_L1 (dimension=5): basic spectral features from GE1 imagery which refers to the mean DN values for every previously segmented object corresponding to the R, G, B, NIR and PAN bands;
- ii) +BGC1 (dimension=5+255): fusion of spectral information and BGC1;
- iii) +CLBP_S_MxC (dimension=5+768): fusion of spectral information and CLBP_S_MxC;
- iv) +CLBP_MxC (dimension=5+512): fusion of spectral information and CLBP_MxC;
- v) +LBP (dimension=5+256): fusion of spectral information and LBP;
- vi) +ILBP (dimension=5+511): fusion of spectral information and ILBP.

Classification and accuracy assessment

First of all, the texture descriptors belonging to GLCM and HEP were individually tested to carry out the supervised classification over the whole working area. The GLCM texture descriptors were totally computed and applied within eCognition environment, whereas the HEP methods were tested by using the aforementioned code implemented in MATLAB®. Later on, the different fusion strategies were also evaluated. The accuracy assessment was always conducted on the same 945 IOs (validation set) by means of the corresponding confusion matrices.

It is important to highlight that the four classes related to buildings (i.e. Red, White, Grey and Other buildings) were grouped in only one class named Buildings before computing the accuracy indexes explained below. Note that the class Buildings was the predominant class within the whole working area, presenting a percentage with respect to the manual classification surface of more than 38% (see Tab. 1).

User's Accuracy (UA), Producer's Accuracy (PA) and Overall Accuracy (OA) were the accuracy values (based on error matrix) computed in this work [Congalton and Green, 2009]. Furthermore, OA is the number of correctly classified objects divided by the total number of objects. Finally, the F_{β} measure [Aksoy et al., 2010], which provides a way of combining UA and PA into a single measure, was also computed according to the Equation [14], where the parameter β determines the weight given to the accuracy computed as PA or UA. The value used in this study ($\beta=1$) weighs UA equal than PA.

$$F_{\beta} = \frac{(\beta^2 + 1) \times PA \times UA}{\beta^2 \times PA + UA} \quad [14]$$

Other important issue to be considered in the classification tasks, mainly when texture features are included and compared, is the required computing budget. In this sense, it is well known that the calculation of GLCM is very computationally intensive and time-consuming, particularly working on high resolution large-size images. For this reason, it is important to evaluate the performance of each texture descriptor in terms of execution time. All the classification experiments carried out in this work were performed on a laptop PC equipped with INTEL® CORE™ i5 CPU 460M, 2.53 GHz, 4 GB RAM, and Windows XP Professional, Service Pack 3.

Statistical analysis

In order to study and compare the influence of factors such as texture descriptors tested and number of training samples on the final classification accuracy, several analysis of variance (ANOVA) tests were carried out by means of a factorial model with four repetitions [Snedecor and Cochran, 1980]. The observed variables were OA, PA, UA, F_{β} , and the execution time. When the results of the ANOVA test turned out to be significant ($p < 0.05$), the separation of means was performed by applying the Duncan's multiple range test at 95% confidence level.

Results and discussion

Pre-Selection of HEP descriptors

The first step in this work was the pre-selection of the HEP descriptors which were going to be further examined. To this end, a one-way ANOVA test over 26 non-parametric texture mappings presented by Fernández et al. [2013] was performed.

Table 3 shows the comparison of mean values for OA attained by the different descriptors working on the 16 training sets. The five finally selected HEP texture descriptors (i.e. LBP, ILBP, BGC1, CLBP_MxC and CLBP_S_MxC shown in bold in Tab. 3) presented OA values better than 67.5% and relatively low dimensions ranging from 255 to 768. All of them had already achieved very good results on the eleven image datasets tested by Fernández et al. [2013]. However, and for the sake of contrasting the results provided in this work, further experiments should be undertaken to assess the performance of all the 26 HEP mappings on other VHR satellite images and other type of land covers.

Table 3 - Overall accuracy (OA) for the 26 non-parametric texture descriptors belonging to the HEP family. OA values followed by different superscript letters indicate significant differences at a significance level $p < 0.05$. The five finally selected HEP texture descriptors are presented in bold.

Name	Acronym	Dimension	OA (%)
Combination completed local binary patterns (S+MxC)	CLBP_S_MxC	768	76.01^a
Combination completed local binary patterns (MxC)	CLBP_MxC	512	72.76^b
Combination completed local binary patterns (SxMxC)	CLBP_SxMxC	131072	71.70 ^{bc}
Improved binary local patterns	ILBP	511	71.13^{cd}
Coordinated clusters representation	CCR	512	69.75 ^{de}
Texture spectrum (0)	TS0	6561	68.97 ^{ef}
Improved binary gradient contours (1)	IBGC1	510	68.92 ^{ef}
Combination completed local binary patterns (SxM)	CLBP_SxM	65536	68.91 ^{ef}
Reduced texture units	RTU	45	68.79 ^{ef}
Local binary patterns	LBP	256	67.93^{fg}
3D Local binary patterns	3DLBP	1024	67.61 ^{fgh}
Binary gradient contours (1)	BGC1	255	67.56^{fgh}
Median binary patterns	MBP	511	67.46 ^{fgh}
Binary gradient contours (2)	BGC2	225	67.14 ^{gh}
Binary texture co-occurrence spectrum	BTCS+	16	66.42 ^{gh}
Grey level texture co-occurrence spectrum	GLTCS+	24	66.23 ^h
Binary gradient contours (3)	BGC3	255	66.21 ^h
Completed local binary patterns (M)	CLBP_M	256	63.12 ⁱ
Gradient-based local binary patterns	GLBP	256	58.41 ^j
Improved center-symmetric local binary patterns (D)	D-LBP	16	55.97 ^k
Improved center-symmetric local binary patterns (ID)	ID-LBP	16	54.36 ^l
Rank transform	RT	9	52.19 ^m
Grey level differences	GLD	256	32.79 ^o
Modified texture spectrum	MTS	16	32.25 ^o
Sum and difference histograms	SDH	4088	30.68 ^p
Simplified texture spectrum	STS	81	30.26 ^p

Table 3 confirms the results found by Fernández et al. [2013], namely that CLBP_S_MxC performs best among the non-parametric HEP methods, presenting an average OA of 76.01%. In addition, the classification accuracy achieved by CLBP_S_MxC is significantly different ($p < 0.05$) with respect to the one computed for the other descriptors (note that the OA value of CLBP_S_MxC in Tab. 3 is followed by the letter “a”, which is not repeated in any other value along it’s the same column). In this way, the OA mean value for CLBP_MxC (72.76%) is not significantly different of the value estimated from CLBP_SxMxC (71.70%), as both values are showing at least one superscript letter in common (in this case the letter “b”).

Comparing single texture descriptors

Once the top ten texture descriptors have been chosen, five belonging to HEP family and five to GLCM, a one-way ANOVA statistic test was carried out to compare their performance. Table 4 shows the corresponding means separation test results (16 repetitions) regarding execution time and OA values for the ten descriptors finally selected. PA and UA values are also indicated, although only for the three most relevant classes (i.e. Building, Shadows and Vegetation).

Regarding execution time, it is worth noting that the GLCM features were significantly ($p < 0.05$) more time-consuming than the HEP ones. In the case of HEP, execution time was clearly related to the dimension of each texture descriptor, being BGC1 and LBP the fastest.

As for the classification accuracy assessment, the five HEP descriptors yielded higher OA values than those based on GLCM, being CLBP_S_MxC the most statistically accurate ($p < 0.05$) texture descriptor. All the Haralick’s texture features computed within eCognition environment achieved poorer OA results. In fact, only GLCM_MEAN presented OA mean values higher than 41%. In that way and working with IKONOS and QuickBird imagery, Musci et al. [2013] have already demonstrated that using LBP descriptors instead of GLCM features may be beneficial for some remote sensing applications.

With regard to PA and UA values computed for the three main target classes, again CLBP_S_MxC performed the best. The HEP descriptors attained very good accuracies figures, especially regarding Shadows and Buildings classes. GLCM_ENT, GLCM_COR, GLCM_STD and GLCM_CON mainly failed over Vegetation and Shadows classes, whereas GLCM_MEAN presented very poor accuracy in the case of Vegetation class.

As it was already reported by Guo et al. [2010], better texture classification accuracy than the state-of-the-art LBP algorithms can be obtained by fusing the CLBP_S, CLBP_M and CLBP_C codes, either in a joint or in a hybrid way. The ranking drawn up by Fernández et al. [2013] presented CLBP_S_MxC as the best texture descriptor of the five HEP mappings tested in this work, followed by ILBP, BGC1, LBP and CLBP_MxC respectively. However, CLBP_MxC was ranked as the second best descriptor according to our results (Tab. 4), indicating that the performance of a texture descriptor can vary depending on the nature of the image where is applied (spatial resolution, image quality, target classes, etc.).

Table 4 - Comparison of mean values for the global ANOVA regarding the execution time, overall accuracy (OA), producer's accuracy (PA) and user's accuracy (UA) for the ten texture descriptors finally selected. Values in the same column followed by different superscript letters indicate significant differences at a significance level $p < 0.05$. The best significant values for each column are presented in bold.

Texture descriptor	Time (s)	OA (%)	Buildings		Shadows		Vegetation	
			PA (%)	UA (%)	PA (%)	UA (%)	PA (%)	UA (%)
GLCM_ENT	543.9 ^f	37.55 ^h	50.44 ^f	53.27 ^e	35.36 ^e	32.53 ^f	12.18 ^d	13.05 ^d
GLCM_COR	651.5 ^g	38.76 ^{gh}	54.63 ^e	54.30 ^e	29.19 ^f	28.60 ^g	18.04 ^{cd}	19.14 ^c
GLCM_SD	522.3 ^e	39.13 ^g	55.15 ^e	53.79 ^e	30.73 ^f	32.95 ^f	15.46 ^{cd}	16.23 ^{cd}
GLCM_CON	528.5 ^e	40.96 ^f	56.51 ^e	57.37 ^d	31.69 ^f	32.08 ^f	19.27 ^c	19.58 ^c
GLCM_MEAN	472.0 ^d	57.77 ^e	70.26 ^d	69.89 ^d	72.70 ^d	72.57 ^e	19.07 ^c	19.95 ^c
BGC1	62.9 ^a	67.56 ^d	76.90 ^{bc}	91.66 ^a	75.29 ^{cd}	82.67 ^c	47.10 ^b	46.00 ^b
LBP	63.9 ^a	67.93 ^d	74.68 ^c	90.51 ^a	77.85 ^c	80.45 ^d	55.93 ^a	45.62 ^b
ILBP	105.8 ^b	71.13 ^c	77.95 ^b	91.45 ^a	81.70 ^b	85.04 ^b	60.18 ^a	46.23 ^b
CLBP_MxC	111.4 ^b	72.76 ^b	81.63 ^a	83.24 ^c	90.06 ^a	86.40 ^b	47.68 ^b	69.04 ^a
CLBP_S_MxC	221.9 ^c	76.01 ^a	83.47 ^a	89.12 ^b	91.11 ^a	89.50 ^a	54.96 ^a	68.30 ^a

Table 5 reports the OA mean values and computation time for each possible combination of texture descriptor and training ratio (i.e. 5%, 10%, 15% and 20%). One can ascertain from the table that computation time is essentially independent of the training ratio for HEP features computed using the MATLAB code we specifically developed for this study. This is so because feature extraction and distance calculation take by far most of the computing time, whereas the contribution of nearest neighbour (1-NN) classification to computation time is negligible. However, and interestingly enough, the computing time shows approximately linear dependence on the training ratio when GLCM features are used and the whole OBIA process is performed within the eCognition environment. This dependency on the training ratio of eCognition computation time might be due to internally implemented optimization procedures which cannot be controlled by the user. On a different note, in general, all the tested descriptors improved their overall classification accuracy from using a larger training set, this fact only was statistically significant ($p < 0.05$) in the case of BGC1 and LBP.

Table 5 - Comparison of mean values regarding execution time and OA for each texture descriptor and training set. Values in the same row followed by different superscript letters indicate significant differences at a significance level $p < 0.05$.

Texture descriptor		5% training	10% training	15% training	20% training
GLCM_ENT	OA (%)	36.62	36.99	38.23	38.36
	Time (s)	230.00 ^d	437.00 ^c	640.83 ^b	867.65 ^a
GLCM_COR	OA (%)	37.88	38.04	39.09	40.02
	Time (s)	272.83 ^d	520.83 ^c	792.83 ^b	1019.40 ^a
GLCM_SD	OA (%)	38.75	38.75	39.44	39.59
	Time (s)	221.23 ^d	412.78 ^c	627.83 ^b	827.30 ^a
GLCM_CON	OA (%)	40.83	40.57	41.81	40.65
	Time (s)	223.23 ^d	429.84 ^c	621.40 ^b	839.70 ^a
GLCM_MEAN	OA (%)	57.33	56.62	58.61	58.83
	Time (s)	197.55 ^d	375.03 ^c	562.25 ^b	753.27 ^a
BGC1	OA (%)	64.81 ^b	67.99 ^a	67.57 ^a	69.89 ^a
	Time (s)	62.92	62.93	62.94	62.94
LBP	OA (%)	66.18 ^b	67.91 ^{ab}	68.26 ^{ab}	69.37 ^a
	Time (s)	63.93	63.93	63.93	63.93
ILBP	OA (%)	70.07	70.18	71.21	73.05
	Time (s)	105.83	105.83	105.83	105.83
CLBP_MxC	OA (%)	70.87	72.55	73.55	74.08
	Time (s)	111.43	111.43	111.44	111.45
CLBP_S_MxC	OA (%)	75.11	75.21	76.76	76.97
	Time (s)	221.93	221.93	221.94	221.95

Comparing fusion strategies

So far, the improvements in terms of computation time and classification accuracy of the HEP texture features, as compared to the GLCM derivatives tested in this work, have already been drawn by using the texture descriptors individually. However, in the field of remote sensing, spectral features may be more important than texture features, and in OBIA classifications, they are always employed together. Henceforth, the improvements regarding the final OBIA classification accuracy due to the potential complementary information added by the texture features to the spectral ones are going to be tested.

In this sense, Table 6 presents the means separation test results from one-way ANOVA (16 repetitions) of OA computed from the different fusion strategies tested. It should be noted that there are two OA values when only the five features corresponding to the spectral

digital values of R, G, B, NIR and PAN bands from the GE1 othoimages were used. One of them was totally computed within eCognition environment (RGBNP_eCog), whereas the other one was carried out by using a MATLAB code (RGBNP_L1). Both approaches employed different NN classifier algorithms, as it was previously explained. In that sense, OA values of around 84% attained by these both methods did not present any significant difference. When the information coming from the GLCM texture descriptors was added to the spectral one by simple concatenation, any improvement in classification accuracy was detected. In fact, the OA results were significantly worse for +5_GLCMs, +GLCM_STD, +GLCM_COR and +GLCM_ENT strategies (values ranging from 81.52% to 82.21%), whereas any remarkable change was obtained by adding +GLCM_MEAN (84.20%) or +GLCM_CON (84.30%). On the other hand, significant improvements with respect to the OA values performed from only spectral features (RGBNP_L1) were achieved when fusing the spectral information and the textural one provided by the HEP descriptors by using the Bayesian criterion. In this case OA values ranging from 84.92% to 86.97% were achieved.

Table 6 - Comparison of mean values regarding overall accuracy (OA), producer's accuracy (PA) and user's accuracy (UA) for the different strategies tested to fuse texture and spectral features. Values in the same column followed by different superscript letters indicate significant differences at a significance level $p < 0.05$. For each column, statistically significant improvement values as compared to both RGBNP_L1 and RGBNP_eCog are presented in bold.

Fusion strategy	OA (%)	Buildings		Shadows		Vegetation	
		PA (%)	UA (%)	PA (%)	UA (%)	PA (%)	UA (%)
+ 5_GLCMs	81.52 ^d	91.45 ^{cde}	89.57 ^{gh}	91.66 ^b	88.00 ^d	65.20 ^e	74.01 ^d
+ GLCM_SD	81.72 ^d	90.67 ^{ef}	88.74 ^h	90.12 ^{bcde}	90.22 ^{bc}	75.00 ^d	81.41 ^c
+ GLCM_COR	81.99 ^d	91.26 ^{def}	90.01 ^{fg}	88.39 ^e	87.50 ^d	77.06 ^{cd}	86.22 ^b
+ GLCM_ENT	82.21 ^d	90.28 ^f	90.61 ^{ef}	89.23 ^{de}	87.25 ^d	75.64 ^d	86.95 ^b
RGBNP_L1	83.93 ^c	92.08 ^{bcd}	90.87 ^{def}	88.70 ^e	91.08 ^{ab}	82.67 ^{ab}	90.37 ^a
RGBNP_eCog	84.16 ^{bc}	92.05 ^{bcd}	91.00 ^{cdef}	89.36 ^{cde}	91.48 ^{ab}	82.86 ^{ab}	89.81 ^a
+ GLCM_MEAN	84.20 ^{bc}	92.14 ^{bcd}	91.10 ^{bcde}	91.84^b	91.39 ^{ab}	79.96 ^{bc}	87.05 ^b
+ GLCM_CON	84.30 ^{bc}	92.51 ^{abc}	90.73 ^{def}	90.35 ^{bcde}	89.62 ^c	80.22 ^{bc}	90.19 ^a
+ BGC1	84.92 ^b	92.33 ^{abcd}	91.96 ^{bc}	91.11 ^{bcd}	91.13 ^{ab}	83.76 ^{ab}	90.46 ^a
+ CLBP_S_MxC	85.00 ^b	92.58 ^{ab}	91.75 ^{bcd}	91.29 ^{bcd}	91.74 ^a	83.38 ^{ab}	90.65 ^a
+ LBP	85.04 ^b	92.31 ^{abcd}	92.13^b	91.50 ^{bc}	91.14 ^{ab}	84.15 ^{ab}	89.90 ^a
+ CLBP_MxC	85.11 ^b	92.72 ^{ab}	91.37 ^{bcde}	91.95^b	92.06 ^a	83.05 ^{ab}	91.49 ^a
+ ILBP	85.12 ^b	92.41 ^{abc}	92.04 ^{bc}	91.50 ^{bc}	91.14 ^{ab}	84.09 ^{ab}	90.27 ^a
+ 5_HEPs	86.97^a	93.28^a	93.48^a	95.42^a	92.19 ^a	84.73 ^a	90.42 ^a

However, the significantly ($p < 0.05$) best overall classification accuracy was achieved by adding the five HEP descriptors to the information contained in the five spectral bands from the GE1 orthoimages (+5_HEPs). For comparison purposes, an overall total extraction accuracy of 80% was observed by Sebari and He [2013] by means of an automatic fuzzy OBIA approach over IKONOS images for urban objects extraction.

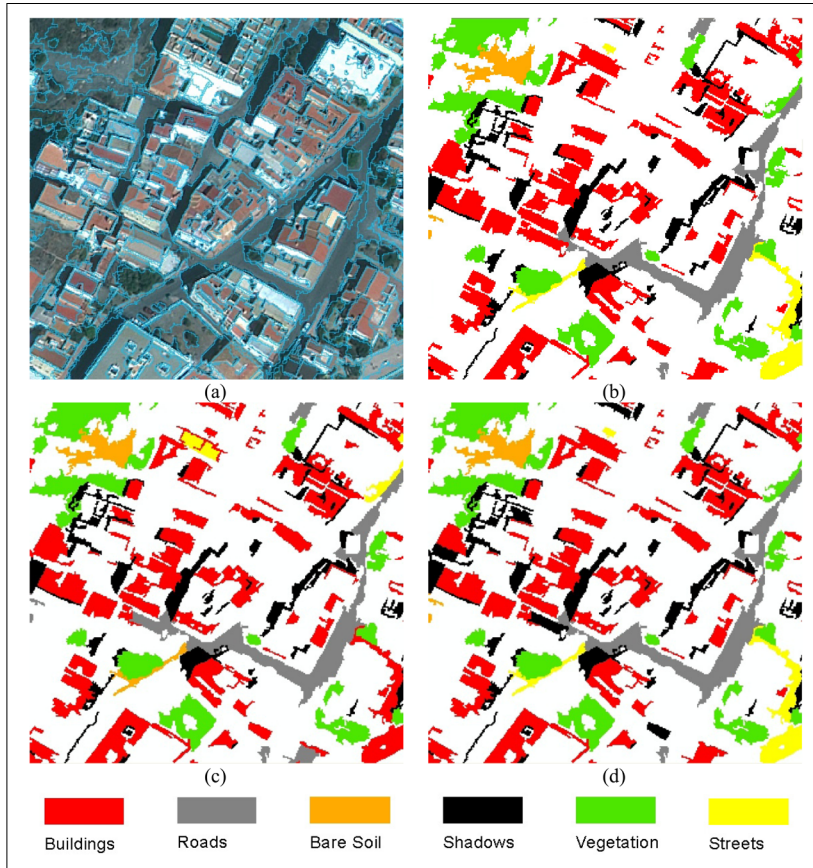


Figure 3 - Detailed results of urban land cover classes on a subarea of 160 m \times 160 m depicting: (a) multiresolution segmentation of GE1 pan-sharpened orthoimage (b) ground truth or validation set (c) classification of the validation IOs from using the fusion strategy + GLCM_MEAN corresponding to the fourth repetition with 20% of training set (d) classification of the validation IOs from using fusion strategy + 5_HEPs for the fourth repetition with 20% of training set.

A qualitative visual evaluation of the classification approaches fusing the spectral and textural information is presented in Figure 3 over a subarea of around 160 m \times 160 m. Also, the performance of the segmentation process can be seen in Figure 3a. The classification results, referred to the IOs belonging to the validation set (Fig. 3b), are presented for the best combinations of GLCM and HEP attained by using the fourth repetition corresponding to the 20% of training size. In this way, + GLCM_MEAN (Fig. 3c) achieved an OA of 85.25%

whereas +5_HEPs reached 89.04% (Fig. 3d). In the case of +5_HEPs combination, the main errors in classification were observed in IOs which should belong to Buildings class but they were misclassified as Shadows. For +GLCM_MEAN case, the misclassification errors was more variable, affecting many classes. In this sense, a good strategy to improve the classification accuracy results in the case of +5_HEPs approach could be to simply carry out a previous IOs classification based on spectral thresholds to extract Shadows objects.

In addition, Table 6 also includes the classification accuracy (PA and UA) for the three most important classes studied (Vegetation, Shadows and Buildings). The different fusion strategies including texture descriptors were not able to significantly improve the accuracy obtained for the Vegetation class (i.e. PA and UA) from only using the spectral features (Tab. 6). This fact is consistent with the results reported by Aguilar et al. [2013] where textures after Haralick were not able to improve vegetation classification accuracy only based on spectral features, neither for GE1 orthoimages nor for WorldView-2 ones. In contrast, Laliberte and Rango [2009] stated that the inclusion of texture measures based on GLCM increased classification accuracies for differentiating rangeland vegetation using OBIA techniques on unmanned aerial vehicles imagery. However, the optimal texture features were not stable, depending so far on the segmentation scales tested.

The results for the classification of vegetation class presented by Aguilar et al. [2013], also corresponding to the GE1 image tested in this work, reached values of 86.1% and 90.1% for PA and UA respectively when employing normalized ratios such as the well-known Normalized Difference Vegetation Index (NDVI) or the Normalized Difference of Blue band Index (NDBI). Notice that these scores were very close to the accuracy results achieved in this work by using the +5_HEPs strategy (Tab. 6).

Regarding Shadows class, three fusion strategies such as +5_HEPs, +CLBP_MxC and +GLCM_MEAN resulted in a statistically significant increase in the PA values with respect to those attained by only using spectral information (Tab. 6). It is well-known that texture features are a potentially powerful method for detecting Shadows as they are highly distinctive, do not depend on colors, and are robust to illumination changes. In fact, the Shadows classification in urban areas has been improved by using textural features based on GLMC as additional information [Su et al., 2008; Aguilar et al., 2013]. However, the accuracy attained by using +5_HEPs was significantly ($p < 0.05$) the best for the Shadows class.

As regards Buildings, +5_HEPs and +LBP strategies managed to significantly increase the accuracy figures only based on spectral features (Tab. 6). Several authors reported that the most relevant feature for classifying Buildings from VHR satellite images turned out to be vertical information from laser scanning [Longbotham et al., 2012; Aguilar et al., 2013]. In that sense, mean values of 94% and 94.6% for PA and UA respectively were reported by Aguilar et al. [2013], working on the same GE1 orthoimages tested in this work, by only using basic spectral features, but adding elevation information from LiDAR data. Contributing with values of 93.28% and 93.48% for PA and UA respectively, the texture information contained in the +5_HEPs strategy tried out in this work was able to almost completely replace the lack of vertical information, which can be considered as a relevant finding.

The classification accuracy of the different fusion strategies was also studied with regard to the size of the training set (Tab. 7). As a general rule, the results turned out to be significantly better ($p < 0.05$) by increasing the percentage of training from 5% to 20%. It is important to note that the expected classification accuracy is related to the training data used, mainly

size and quality [Foody and Mathur, 2006]. Although all the fusion strategies involving HEP descriptors achieved OA values higher than the benchmark set up from only spectral information, statistically significant improvements were only attained by using +5_HEPs on the training sets ranging from 10% to 20%. Conversely, and in statistic terms, strategies involving GLCM derivatives did not improve the classification accuracy achieved from only the spectral information.

Table 7 - Comparison of mean OA values for the different fusion strategies and training size. Values in the same row followed by different superscript letters indicate significant differences at a significance level $p < 0.05$. Different subscript letters within the same column indicate significant differences ($p < 0.05$). For each column, statistically significant improvement values as compared to both RGBNP_L1 and RGBNP_eCog are presented in bold.

Fusion strategy	Overall Accuracy (%)			
	5% training	10% training	15% training	20% training
RGBNP_eCog	83.06 ^b _{abc}	83.48 ^b _{bc}	84.33 ^{ab} _b	85.77 ^a _{bc}
+ GLCM_ENT	80.85 ^b _{bcd}	82.19 ^{ab} _{cd}	82.75 ^{ab} _c	83.04 ^a _d
+ GLCM_COR	79.48 ^b _d	82.33 ^a _{cd}	82.48 ^a _c	83.67 ^a _d
+ GLCM_SD	80.32 ^b _{cd}	81.27 ^{ab} _d	82.72 ^a _c	82.59 ^a _d
+ GLCM_CON	82.85 ^b _{abc}	84.12 ^{ab} _b	84.91 ^{ab} _b	85.33 ^a _c
+ GLCM_MEAN	82.48 ^b _{abc}	84.09 ^{ab} _b	84.51 ^a _b	85.72 ^a _{bc}
+ 5_GLCMs	79.56 ^b _d	81.35 ^{ab} _d	82.48 ^a _c	82.69 ^a _d
RGBNP_L1	82.62 ^b _{abc}	83.30 ^b _{bc}	84.72 ^{ab} _b	85.36 ^a _{bc}
+ BGC1	83.75 ^b _{ab}	84.46 ^b _b	85.22 ^{ab} _b	86.25 ^a _{bc}
+ LBP	83.69 ^b _{ab}	84.59 ^{ab} _b	85.41 ^{ab} _b	86.49 ^a _{bc}
+ ILBP	83.74 ^b _{ab}	84.64 ^{ab} _b	85.57 ^{ab} _b	86.51 ^a _{bc}
+ CLBP_MxC	83.61 ^b _{ab}	84.51 ^b _b	85.59 ^{ab} _b	86.72 ^a _b
+ CLBP_S_MxC	83.59 ^b _{ab}	84.22 ^b _b	85.46 ^{ab} _b	86.73 ^a _b
+ 5_HEPs	85.01 ^c _a	86.91^b_a	87.39^{ab}_a	88.57^a_a

The larger training set size and the more consistent repetitions usually imply that the results can be analyzed in a better way. Therefore, Table 8 shows the classification accuracy in terms of F_{β} for each target class by grouping the results corresponding to the 15% and 20% training sets, therefore using eight repetitions in the ANOVA statistic test. There was a clear trend to improve the classification accuracy achieved from only spectral features when using HEP texture descriptors for all the target classes with the exception of Vegetation.

However, the best and statistically significant values of F_{β} were only attained for the +5_ HEPs strategy and the classes named as Buildings, Shadows and Bare Soil. The +CLBP_ MxC approach also yielded significantly better accuracy in terms of F_{β} when it was applied to classify the Shadows class.

Table 8 - Comparison of mean F_{β} values for each class and different fusion strategies by groping the training repetitions of 15% and 20%. Values in the same column followed by different superscript letters indicate significant differences at a significance level $p < 0.05$. For each column, statistically significant improvement values as compared to both RGBNP_L1 and RGBNP_eCog are presented in bold.

Fusion strategy	F_{β} (%) Buildings	F_{β} (%) Shadows	F_{β} (%) Vegetation	F_{β} (%) Roads	F_{β} (%) Bare Soil	F_{β} (%) Streets
RGBNP_eCog	91.84 ^{bc}	91.28 ^{cdef}	87.71 ^a	53.97 ^{abc}	42.19 ^b	37.13 ^{ab}
+ GLCM_ENT	90.76 ^{de}	88.85 ^g	82.31 ^{cd}	46.82 ^d	39.00 ^{bc}	36.32 ^{ab}
+ GLCM_COR	91.07 ^{cde}	89.01 ^g	84.17 ^{bc}	46.10 ^{de}	36.19 ^c	31.03 ^{bc}
+ GLCM_SD	90.11 ^{de}	90.99 ^{def}	80.72 ^d	40.99 ^{ef}	39.44 ^{bc}	26.26 ^c
+ GLCM_CON	91.95 ^{bc}	90.39 ^f	87.15 ^a	51.07 ^{bcd}	40.78 ^{bc}	40.80 ^a
+ GLCM_MEAN	92.05 ^{bc}	92.73 ^b	85.16 ^b	50.34 ^{cd}	38.73 ^{bc}	35.11 ^{ab}
+ 5_GLCMs	90.80 ^{de}	91.13 ^{def}	72.81 ^c	38.86 ^f	36.04 ^c	37.05 ^{ab}
RGBNP_L1	91.76 ^{bcd}	90.89 ^{ef}	88.42 ^a	54.91 ^{abc}	40.29 ^{bc}	36.15 ^{ab}
+ BGC1	92.48 ^b	91.64 ^{cde}	88.32 ^a	56.29 ^{abc}	42.71 ^b	38.44 ^{ab}
+ LBP	92.59 ^b	91.96 ^{bcde}	88.42 ^a	56.59 ^{abc}	43.06 ^b	38.38 ^{ab}
+ ILBP	92.58 ^b	92.02 ^{bcd}	88.53 ^a	57.05 ^{ab}	43.47 ^b	37.98 ^{ab}
+ CLBP_MxC	92.51 ^b	92.74^b	89.17 ^a	55.74 ^{abc}	42.79 ^b	38.19 ^{ab}
+ CLBP_S_MxC	92.62 ^b	92.27 ^{bc}	88.90 ^a	56.40 ^{abc}	44.04 ^b	37.24 ^{ab}
+ 5_HEPs	93.80^a	94.34^a	88.60 ^a	59.24 ^a	51.18^a	42.72 ^a

Conclusions

In this paper, 26 non-parametric texture descriptors which characterize a texture image through the probability of occurrence of the patterns associated to a neighborhood of given size and shape (Histograms of Equivalent Patterns, HEP) has been tested. Most of these HEP descriptors were originally developed in the fields of computer vision and pattern recognition and, to our best knowledge, many of them had never been used in VHR satellite imagery classification. The HEP descriptors have been compared with the widely used texture measures derived from the gray-level co-occurrence matrix (GLCM) in order to improve urban land-use mapping by applying OBIA supervised classification (NN) from GE1 orthoimages.

The classification assessment carried out only involving single texture features proved that any of the five best tested HEP descriptors (i.e., LBP, ILBP, BGC1, CLBP_MxC and CLBP_S_MxC) significantly ($p < 0.05$) improved the results achieved from the GLCM approaches (i.e., CON, ENT, MEAN, STD and COR), both in terms of accuracy and computation time. In the case of HEP descriptors, the higher was the dimension of each descriptor, the longer was the execution time. Regarding the accuracy results, whereas values of OA ranging from 37.5% to 57.8% were attained by using GLCM features, much better OA figures ranging from 67.5% to 76% were achieved through HEP descriptors.

Nevertheless, the clear advantages of the HEP-based texture measures stated above only would have any sense in remote sensing if they were able to add extra information to the spectral feature vector from GE1 imagery (R, G, B, NIR and PAN bands). It is noted that in the field of remote sensing, spectral and texture features are both always considered together. In this way, statistically significant ($p < 0.05$) improvements in overall accuracy figures of around 3% (achieving values of up to 88.57%) were attained when the fusion strategy (Bayesian Average scheme) involving the five HEP texture descriptors was used. Conversely, and in statistic terms, strategies involving GLCM derivatives did not improve the classification accuracy achieved from only spectral information. Regarding the size of the training set for NN supervised classification, both approaches (HEP and GLCM) showed similar behavior.

These findings related to the application of HEP texture descriptors on VHR remote sensing imagery are quite promising, but they should be contrasted in further works by being applied on other VHR satellite imagery and other non-urban areas. Also, it would be very interesting to test the performance of other parametric and non-parametric texture measures belonging to the HEP family.

The last but not the least, the problem of the high dimension of HEP mappings as compared to the low dimension of the spectral feature vector for GE1 would be solved to features fusion purposes. In our case, a fusion of a-posteriori class probabilities through Bayesian average was proposed, but this method could be improved and even adapted for other classifier.

Acknowledgements

This work was supported by the Spanish Ministry of Economy and Competitiveness (Spain) and the European Union (FEDER funds) under Grant References AGL2014-56017-R and CTM2010-16573. It takes part of the general research lines promoted by the Agrifood Campus of International Excellence ceiA3, <http://www.ceia3.es/>. The authors would like to thank anonymous reviewers for their constructive comments on earlier drafts of this manuscript.

References

- Aguera F., Aguilar F.J., Aguilar M.A. (2008) - *Using texture analysis to improve per-pixel classification of very high resolution images for mapping plastic greenhouses*. ISPRS Journal of Photogrammetry and Remote Sensing, 63: 635-646. doi: <http://dx.doi.org/10.1016/j.isprsjprs.2008.03.003>.
- Aguilar M.A., Aguilar F.J., Saldaña M.M., Fernández I. (2012) - *Geopositioning Accuracy Assessment of GeoEye-1 Panchromatic and Multispectral Imagery*. Photogrammetric

- Engineering and Remote Sensing, 78 (3): 7181-7197. doi: <http://dx.doi.org/10.14358/pers.78.3.247>.
- Aguilar M.A., Saldaña M.M., Aguilar F.J. (2013) - *GeoEye-1 and WorldView-2 pan-sharpened imagery for object-based classification in urban environments*. International Journal of Remote Sensing, 34 (7): 2583-2606. doi: <http://dx.doi.org/10.1080/01431161.2012.747018>.
- Aksoy S., Akcay H.G., Wassenaar T. (2010) - *Automatic mapping of linear woody vegetation features in agricultural landscapes using very high-resolution imagery*. IEEE Transactions on Geoscience and Remote Sensing, 48 (1): 511-522. doi: <http://dx.doi.org/10.1109/TGRS.2009.2027702>.
- Baatz M., Benz U., Dehghani S., Heynen M., Höltje A., Hofmann P., Lingenfelder I., Mimler M., Sohlbach M., Weber M., Willhauck G. (2004) - *eCognition elements user guide 4.0*. München, Germany: Definiens Imaging GmbH.
- Baraldi A., Pannigiani F. (1995) - *An Investigation of the Textural Characteristics Associated with Gray Level Cooccurrence Matrix Statistical Parameters*. IEEE Transactions on Geoscience and Remote Sensing, 33 (2): 293-304. doi: <http://dx.doi.org/10.1109/36.377929>.
- Blaschke T. (2010) - *Object Based Image Analysis for Remote Sensing*. ISPRS Journal of Photogrammetry and Remote Sensing, 65 (1): 2-16. doi: <http://dx.doi.org/10.1016/j.isprsjprs.2009.06.004>.
- Bianconi F., Fernández A. (2007) - *Evaluation of the effects of Gabor filter parameters on texture classification*. Pattern Recognition, 40: 3325-3335. doi: <http://dx.doi.org/10.1016/j.patcog.2007.04.023>.
- Bianconi F., Fernández A. (2014) - *A unifying framework for LBP and related methods*. In: Local Binary Patterns: New Variants and Applications (Studies in Computational Intelligence), Springer, pp. 17-46. doi: http://dx.doi.org/10.1007/978-3-642-39289-4_2.
- Carleer A.P., Wolff E. (2006) - *Urban land cover multi-level region-based classification of VHR data by selecting relevant features*. International Journal of Remote Sensing, 27 (6): 1035-1051. doi: <http://dx.doi.org/10.1080/01431160500297956>.
- Clausi D.A., Deng H. (2005) - *Design-based texture feature fusion using Gabor filters and co-occurrence probabilities*. IEEE Transactions on Image Processing, 14 (7): 925-936. doi: <http://dx.doi.org/10.1109/TIP.2005.849319>.
- Congalton R.G., Green K. (2009) - *Assessing the Accuracy of Remotely Sensed Data: Principles and Practices*. 2nd Ed. Boca Raton, FL: CRS Press/Taylor & Francis.
- Definiens (2009) - *Definiens eCognition Developer 8 Reference Book*. München: Definiens AG.
- Deselaers T., Heigold G., Ney H. (2010) - *Object classification by fusing SVMs and Gaussian mixtures*. Pattern Recognition, 43 (7): 2476-2484. doi: <http://dx.doi.org/10.1016/j.patcog.2010.02.002>.
- Eckert S. (2012) - *Improved forest biomass and carbon estimations using texture measures from WorldView-2 satellite data*. Remote Sensing, 4 (4), 810-829. doi: <http://dx.doi.org/10.3390/rs4040810>.
- Fernández A., Álvarez M.X., Bianconi F. (2011) - *Image classification with binary gradient contours*. Optics and Lasers in Engineering, 49 (9-10): 1177-1184. doi: <http://dx.doi.org/10.1016/j.optlaseng.2011.05.003>.

- Fernández A., Álvarez M.X., Bianconi F. (2013) - *Texture description through Histograms of Equivalent Patterns*. Journal of Mathematical Imaging and Vision, 45: 76-102. doi: <http://dx.doi.org/10.1007/s10851-012-0349-8>.
- Ferro C.J.S., Warner T.A. (2002) - *Scale and texture in digital image classification*. Photogrammetric Engineering and Remote Sensing, 68: 51-63.
- Foody G.M., Mathur A. (2006) - *The use of small training sets containing mixed pixels for accurate hard image classification: Training on mixed spectral responses for classification by a SVM*. Remote Sensing of Environment, 103 (2): 179-189. doi: <http://dx.doi.org/10.1016/j.rse.2006.04.001>.
- Gianinetto M., Rusmini M., Candiani G., Dalla Via, G., Frassy F., Maianti P., Marchesi A., Rota Nodari F., Dini L. (2014) - *Hierarchical classification of complex landscape with VHR pan-sharpened satellite data and OBIA techniques*. European Journal of Remote Sensing, 47: 229-250. doi: <http://dx.doi.org/10.5721/EuJRS20144715>.
- Guo Z., Zhang L., Zhang D. (2010) - *A completed modeling of Local Binary Pattern operator for texture classification*. IEEE Transactions on Image Processing, 19 (6): 1657-1663. doi: <http://dx.doi.org/10.1109/TIP.2010.2044957>.
- Haralick R.M., Shanmugam K., Dinstein I.H. (1973) - *Textural features for image classification*. IEEE Transactions on Systems, Man and Cybernetics, 3 (6): 610-621. doi: <http://dx.doi.org/10.1109/TSMC.1973.4309314>.
- Huang X., Zhang L. (2012) - *A multiscale urban complexity index based on 3D wavelet transform for spectral-spatial feature extraction and classification: an evaluation on the 8-channel WorldView-2 imagery*. International Journal of Remote Sensing, 33 (8): 2641-2656. doi: <http://dx.doi.org/10.1080/01431161.2011.614287>.
- Jin H., Liu Q., Lu H., Tong X. (2004) - *Face detection using improved LBP under Bayesian framework*. Proceedings of the 3rd International Conference on Image and Graphics (ICIG), Hong Kong, China, 306-309.
- Kittler J., Hatef M., Duin R.P.W., Matas J. (1998) - *On combining classifiers*. IEEE Transactions Pattern Analysis and Machine Intelligence, 20 (3): 226-239. doi: <http://dx.doi.org/10.1109/34.667881>.
- Laliberte A.S., Rango A. (2009) - *Texture and scale in object-based analysis of subdecimeter resolution Unmanned Aerial Vehicle (UAV) imagery*. IEEE Transactions on Geoscience and Remote Sensing, 47 (3): 761-770. doi: <http://dx.doi.org/10.1109/TGRS.2008.2009355>.
- Li M., Zang S., Zhang B., Li S., Wu C. (2014) - *A Review of Remote Sensing Image Classification Techniques: the Role of Spatio-contextual Information*. European Journal of Remote Sensing, 47: 389-411. doi: <http://dx.doi.org/10.5721/EuJRS20144723>.
- Li W., Chen C., Su H., Du Q. (2015) - *Local Binary Patterns and Extreme Learning Machine for Hyperspectral Imagery Classification*. IEEE Transactions on Geoscience and Remote Sensing, 53 (7): 3681-3693. doi: <http://dx.doi.org/10.1109/TGRS.2014.2381602>.
- Li Z., Hayward R., Zhang J., Jin H., Walker R. (2010) - *Evaluation of spectral and texture features for object-based vegetation species classification using support vector machines*. Proceedings of the International Archives of the Photogrammetry, Remote Sensing and Spatial Information Sciences, XXXVIII (7A), ISPRS TC VII Symposium, Vienna, Austria.
- Longbotham N., Chaapel C., Bleiler L., Padwick C., Emery W.J., Pacifici F. (2012) -

- Very High Resolution multiangle urban classification analysis*. IEEE Transactions on Geoscience and Remote Sensing, 50 (4): 1155-1170. doi: <http://dx.doi.org/10.1109/TGRS.2011.2165548>.
- Lorette A., Descombes X., Zerubia J. (2000) - *Texture analysis through a Markovian modelling and fuzzy classification: Application to urban area extraction from satellite images*. International Journal of Computer Vision, 36 (3): 221-236. doi: <http://dx.doi.org/10.1023/A:1008129103384>.
- Lu D., Hetrick S., Moran E. (2010) - *Land Cover classification in a complex urban-rural landscape with QuickBird imagery*. Photogrammetric Engineering and Remote Sensing, 76 (10): 1159-1168. doi: <http://dx.doi.org/10.14358/PERS.76.10.1159>.
- Lucieer A., Stein A., Fisher P. (2005) - *Multivariate texture-based segmentation of remotely sensed imagery for extraction of objects and their uncertainty*. International Journal of Remote Sensing, 26(4): 2917-2936. doi: <http://dx.doi.org/10.1080/01431160500057723>.
- Malek S., Bazi Y., Alajlan N., AlHichri H., Melgani F. (2014) - *Efficient Framework for Palm Tree Detection in UAV Images*. IEEE Journal of Selected Topics in Applied Earth Observations and Remote Sensing, 7 (12): 4692- 4703. doi: <http://dx.doi.org/10.1109/JSTARS.2014.2331425>.
- Marpu P.R., Neubert M., Herold H., Niemeyer I. (2010) - *Enhanced evaluation of image segmentation results*. Journal of Spatial Science, 55 (1): 55-68. doi: <http://dx.doi.org/10.1080/14498596.2010.487850>.
- Mdakane L., Van den Bergh F. (2012) - *Extended local binary pattern features for improving settlement type classification of QuickBird images*. PRASA 2012: Twenty-Third Annual Symposium of the Pattern Recognition Association of South Africa, Pretoria, South Africa, 29-30 November 2012.
- Myint S.W., Lam N.S.N., Tyler J.M. (2004) - *Wavelets for urban spatial feature discrimination: comparisons with fractal, spatial autocorrelation, and spatial co-occurrence approaches*. Photogrammetric Engineering and Remote Sensing, 70 (7): 803-812. doi: <http://dx.doi.org/10.14358/PERS.70.7.803>.
- Myint S.W., Gober P., Brazel A., Grossman-Clarke S., Weng Q. (2011) - *Per-pixel vs. object-based classification of urban land cover extraction using high spatial resolution imagery*. Remote Sensing of Environment, 115 (5): 1145-1161. doi: <http://dx.doi.org/10.1016/j.rse.2010.12.017>.
- Murray H., Lucieer A., Williams R. (2010) - *Texture-based classification of sub-Antarctic vegetation communities on Heard Island*. International Journal of Applied Earth Observation and Geoinformation, 12 (3): 138-149. doi: <http://dx.doi.org/10.1016/j.jag.2010.01.006>.
- Musci M., Queiroz Feitosa R., Costa G.A.O.P., Fernandes Velloso M.L. (2013) - *Assessment of Binary Coding Techniques for Texture Characterization in Remote Sensing Imagery*. IEEE Geoscience and Remote Sensing Letters, 10 (6): 1607-1611. doi: <http://dx.doi.org/10.1109/LGRS.2013.2267531>.
- Nikolakopoulos K., Oikonomidis D. (2015) - *Quality assessment of ten fusion techniques applied on Worldview-2*. European Journal of Remote Sensing, 48: 141-167. doi: <http://dx.doi.org/10.5721/EuJRS20154809>.
- Ojala T., Pietikäinen M., Mäenpää T.T. (2002) - *Multiresolution gray-scale and rotation invariant texture classification with local binary pattern*. IEEE Transactions on Pattern

- Analysis and Machine Intelligence, 24 (7): 971-987. doi: <http://dx.doi.org/10.1109/TPAMI.2002.1017623>.
- Ozdemir I., Karnieli A. (2011) - *Predicting forest structural parameters using the image texture derived from WorldView-2 multispectral imagery in a dryland forest, Israel*. International Journal of Applied Earth Observation and Geoinformation, 13 (5): 701-710. doi: <http://dx.doi.org/10.1016/j.jag.2011.05.006>.
- Parrinello T., Vaughan R.A. (2002) - *Multifractal analysis and feature extraction in satellite imagery*. International Journal of Remote Sensing, 23 (9): 1799-1825. doi: <http://dx.doi.org/10.1080/01431160110075820>.
- Permuter H., Francos J., Jermyn I. (2006) - *A study of Gaussian mixture models of color and texture features for image classification and segmentation*. Pattern Recognition, 39 (4): 695-706. doi: <http://dx.doi.org/10.1016/j.patcog.2005.10.028>.
- Puissant A., Hirsch J., Weber C. (2005) - *The utility of texture analysis to improve per-pixel classification for high to very high spatial resolution imagery*. International Journal of Remote Sensing, 26(4): 733-745. doi: <http://dx.doi.org/10.1080/01431160512331316838>.
- Ruta D., Gabrys B. (2000) - *An overview of classifier fusion methods*. Computing and Information Systems, 7: 1-10.
- Sarp G. (2014) - *Spectral and spatial quality analysis of pan-sharpening algorithms: A case study in Istanbul*. European Journal of Remote Sensing, 47: 19-28. doi: <http://dx.doi.org/10.5721/EuJRS20144702>.
- Sebari I., He D.-C. (2013) - *Automatic fuzzy object-based analysis of VHRS images for urban objects extraction*. ISPRS Journal of Photogrammetry and Remote Sensing, 79: 171-184. doi: <http://dx.doi.org/10.1016/j.isprsjprs.2013.02.006>.
- Segl K., Roessner S., Heiden U., Kaufmann H. (2003) - *Fusion of spectral and shape features for identification of urban surface cover types using reflective and thermal hyperspectral data*. ISPRS Journal of Photogrammetry and Remote Sensing, 58 (1-2): 99-112. doi: [http://dx.doi.org/10.1016/S0924-2716\(03\)00020-0](http://dx.doi.org/10.1016/S0924-2716(03)00020-0).
- Snedecor G.W., Cochran W.G. (1980) - *Statistical Methods. 7th ed.* Ames, IA: Iowa State University Press.
- Stumpf A., Kerle N. (2011) - *Object-oriented mapping of landslides using Random Forests*. Remote Sensing of Environment, 115 (10): 2564-2577. doi: <http://dx.doi.org/10.1016/j.rse.2011.05.013>.
- Su H., Yong B., Du P., Liu H., Chen C., Liu K. (2014) - *Dynamic classifier selection using spectral-spatial information for hyperspectral image classification*. Journal of Applied Remote Sensing, 8 (1): 085095. doi: <http://dx.doi.org/10.1117/1.JRS.8.085095>.
- Su H., Sheng Y., Du P., Chen C., Liu K. (2015) - *Hyperspectral image classification based on volumetric texture and dimensionality reduction*. Frontiers of Earth Science, 9 (2): 225-236. doi: <http://dx.doi.org/10.1007/s11707-014-0473-4>.
- Su W., Li J., Chen Y., Liu Z., Zhang J., Low T.M., Inbaraj S., Siti A.M.H. (2008) - *Textural and local spatial statistics for the object-oriented classification of urban areas using high resolution imagery*. International Journal of Remote Sensing, 29 (11): 3105-3117. doi: <http://dx.doi.org/10.1080/01431160701469016>.
- Tsai F., Chang, C.K., Rau, J.Y., Lin, T.H., Liu G.R. (2007) - *3D computation of gray level co-occurrence in hyperspectral image cubes*. Lecture Notes in Computer Science, 4679: 429-440. doi: http://dx.doi.org/10.1007/978-3-540-74198-5_33.

Weng Q. (2012) - *Remote sensing of impervious surfaces in the urban areas: requirements, methods, and trends*. Remote Sensing of Environment, 117: 34-49. doi: <http://dx.doi.org/10.1016/j.rse.2011.02.030>.

Zhao Y., Zhang L., Li P., Huang B. (2007) - *Classification of high spatial resolution imagery using improved Gaussian Markov random-field-based texture features*. IEEE Transactions on Geoscience and Remote Sensing, 45 (5): 1458-1468. doi: <http://dx.doi.org/10.1109/TGRS.2007.892602>.

© 2016 by the authors; licensee Italian Society of Remote Sensing (AIT). This article is an open access article distributed under the terms and conditions of the Creative Commons Attribution license (<http://creativecommons.org/licenses/by/4.0/>).